Biogeosciences Discuss., 9, 9945–9991, 2012
www.biogeosciences-discuss.net/9/9945/2012/
doi:10.5194/bgd-9-9945-2012

Biogeosciences Discussions

Carbon dioxide balance of subarctic tundra from plot to regional scales

M. E. Marushchak[1,3], I. Kiepe[2], C. Biasi[1], V. Elsakov[3], T. Friborg[2], T. Johansson[2], H. Soegaard[2], T. Virtanen[4], and P. J. Martikainen[1]

[1]Department of Environmental Science, University of Eastern Finland, P.O. Box 1627, 70211 Kuopio, Finland
[2]Department of Geography & Geology, University of Copenhagen, Øster Voldgade 10, 1350 Copenhagen K, Denmark
[3]Institute of Biology, Komi SC UrD RAS, 167982 Syktyvkar, Russia
[4]Department of Environmental Sciences, University of Helsinki, P.O. Box 27, 00014 University of Helsinki, Finland

Received: 25 June 2012 – Accepted: 12 July 2012 – Published: 1 August 2012

Correspondence to: M. E. Marushchak (maija.marushchak@uef.fi)

Published by Copernicus Publications on behalf of the European Geosciences Union.

Abstract

We report here the carbon dioxide (CO_2) budget of a 98.6-km^2 subarctic tundra area in Northeast European Russia based on measurements at two different scales and two independent up-scaling approaches. Plot scale measurements (chambers on terrestrial surfaces, gas gradient method and bubble collectors on lakes) were carried out from July 2007 to October 2008. The landscape scale eddy covariance (EC) measurements covered the snow-free period 2008. The annual net ecosystem exchange (NEE) of different land cover types ranged from −251 to 84 g C m^{-2}. Leaf area index (LAI) was an excellent predictor of the spatial variability in gross photosynthesis (GP), NEE and ecosystem respiration (ER). The plot scale CO_2 fluxes were first scaled up to the EC source area and then to the whole study area using two data sets: a land cover classification and a LAI map, both based on field data and 2.4 m pixel-sized Quickbird satellite image. The good agreement of the CO_2 balances for the EC footprint based on the different methods (−105 to −81 g C m^{-2} vs. −79 g C m^{-2}; growing season 2008) justified the integration of the plot scale measurements over the larger area. The annual CO_2 balance for the study region was −67 to −41 g C m^{-2}. Due to the heterogeneity of tundra, the effect of climate change on CO_2 uptake will vary strongly according to the land cover type and, moreover, likely changes in their relative coverage in future will have great impact on the regional CO_2 balance.

1 Introduction

The strong warming predicted for the Arctic by global climate models (IPCC, 2007) has underlined the need to understand how carbon (C) fluxes in tundra will respond to climate change. Carbon storage in plant biomass is low in the Arctic (Bazilevich, 1993; Hugelius et al., 2011), but northern permafrost soils contain as much as 50 % of global belowground soil C pool (Tarnocai et al., 2009). There, higher temperatures and permafrost thaw will likely enhance the mineralization of soil organic matter in future,

BGD
9, 9945–9991, 2012

thereby increasing release of C as carbon dioxide (CO_2) to the atmosphere (Dorrepaal et al., 2009; Schuur et al., 2009). At the same time, there will be changes in vegetation composition and productivity (Walker et al., 2006; Forbes et al., 2010), and the increase in above ground C stocks may partly compensate for the respiratory below ground C losses at least in the short term (Qian et al., 2010).

In order to predict the changes in the tundra C balance in the future, we need to accurately estimate the present-day C balance and understand its dependence on environmental factors. This is a real challenge, taking into account the high temporal (e.g., Kwon et al., 2006; Groendahl et al., 2007) and spatial (e.g., Heikkinen et al., 2004; Fox et al., 2008) variability of CO_2 fluxes in tundra, as well as the logistical difficulties when working in remote areas. Studies on tundra CO_2 exchange have been previously conducted using either micrometeorological eddy covariance (EC) method (e.g., Moncrieff et al., 1997; Nordstroem et al., 2001; Corradi et al., 2005; Kutzbach et al., 2007b; Lafleur and Humphreys, 2008; Humphreys and Lafleur, 2011; Parmantier et al., 2011; Lund et al., 2012) or chamber techniques (e.g., Christensen et al., 2000; Heikkinen et al., 2002, 2004; Shaver et al., 1998, 2007). Although the EC and chamber methods are complementary for each other, there are only few studies where these two techniques are applied in parallel in CO_2 exchange studies in tundra (Soegaard et al., 2003; Zamolodchikov et al., 2003; Fox et al., 2008).

With high-frequency micrometeorological EC measurements it is possible to get continuous data set over a source area of 0.1–1 km^2 and catch the short-term variations in gas fluxes often missed by (manual) chambers (e.g., Pihlatie et al., 2010). On the other hand, chamber measurements give information on spatial variability in fluxes of different functional ecosystem types, often located at short distance in tundra landscape. This kind of data provides good grounds for extrapolating, or "up-scaling" fluxes to a regional scale. However, up-scaling based on chambers can be risky if the measuring frequency is low or the distribution of various surfaces is not well-documented. Chamber measurements can also cause disturbance to the studied system and, thus, affect the gas flux rates observed (e.g., Kutzbach et al., 2007a). In the up-scaling process,

BGD
9, 9945–9991, 2012

comparison of EC results and plot scale measurements in the EC source area serves as an intermediate step towards extrapolation to larger scale, making the regional estimates scientifically sound.

Due to the fragmented nature of tundra environment, it is critical to select a relevant spatial scale for up-scaling efforts. Landsat satellite data with 30 m resolution, used in most studies on regional CO_2 balance of tundra (Soegaard et al., 2003; Heikkinen et al., 2004), are not detailed enough to detect the smaller scale differences typical for tundra (Laidler and Treitz, 2003). First remote sensing studies on Arctic vegetation using higher resolution than Landsat satellite images have been conducted only recently (Fuchs et al., 2009). In the present study, we use a land cover classification (LCC) based on QuickBird imagery with 2.4 m resolution, appropriate for detecting the relevant spatial variability of the landscape investigated.

In this study, we aimed at quantifying CO_2 fluxes in a tundra landscape and investigating the controlling factors, in order to provide a sound basis for up-scaling the fluxes to the regional level. The study was conducted in discontinuous permafrost region in Komi Republic, Northern European Russia. We measured the CO_2 exchange over a whole snow-free period at two different scales: the chamber technique in terrestrial surfaces and the gas gradient method and bubble traps in lakes (plot scale), and the EC method (landscape scale). The results of these methods were compared in the EC source area using the footprint analysis. Plot measurements, conducted over a prolonged period (two summers and one winter), give insights to the inter- and intra-annual variability in CO_2 exchange. The final goal was to estimate the CO_2 balance for a region of 98.6 km^2 based on the fluxes of different land cover types (LCTs) that were scaled up using two high-resolution satellite derived data sets, LCC and leaf area index (LAI) map.

BGD
9, 9945–9991, 2012

2 Methods

2.1 Study site

The study site, near the settlement Seida, is located in southern tundra with discontinuous permafrost in Northeast European Russia (67°03′ N, 62°56′ E). The mean air temperature in the region is −5.6 °C and the mean annual precipitation 501 mm. Monthly mean values are found in Table 1 (long-term averages for 1977–2006, data from Vorkuta station (67°48′ N, 64°01′ E, 172 m a.s.l.); Komi Republican Center for Hydrometeorological and Environmental Monitoring).

Most of the landscape in the region is hilly upland with tundra heath vegetation ("Upland tundra"; coverage 58 %) dominated by shrub-lichen-moss communities (Table 2). Also peatlands with bog vegetation are typical for the region ("Dry peatlands"; coverage 24 %). These peatlands include peat plateaus with up to several meters thick peat deposits, raised up by permafrost. The peat plateaus are spotted by unvegetated patterned ground features ("Bare peat") and small thermokarst lakes ("Lakes"). Narrow fens and willow stands ("Wetlands"; 14 %) are located on low-lying parts of the landscape that act as water conduits in the terrain. The above-mentioned LCTs, all studied at plot scale (Table 2), represent 97 % of the landscape. The residual landscape area (3 %) is covered by deciduous and coniferous forest stands, rivers, human-impacted tundra and sand. The terrestrial microsites and lakes studied at the plot-scale were located within the EC footprint area North-East from the EC tower (Fig. 1a). More details on the soils and vegetation at the Seida study site are provided by Hugelius et al. (2011) and Marushchak et al. (2011).

2.2 Auxiliary data

Auxiliary data was collected on air temperature, soil heat flux, net radiation, photosynthetically active radiation (PAR), precipitation, wind speed, soil moisture (θ_v), soil temperature, leaf area index and active layer depth. The leaf area index of vascular

BGD
9, 9945–9991, 2012

plants (LAI) was measured in June–September 2008 at 284 field measurement points (Fig. 1b). More details on auxiliary data collection are available in Supplement.

2.3 Carbon dioxide exchange at plot scale

2.3.1 Chamber measurements at terrestrial microsites

Exchange of CO_2 was measured at the terrestrial microsites with a closed chamber technique (Heikkinen et al., 2002) in July–October 2007 and May–October 2008. Measurements were carried out mainly between 08:00 a.m. and 09:00 p.m. using a transparent polycarbonate chamber (30 × 60 × 60 cm) with an infra-red gas analyzer (Li-840, LiCor). The chamber had a cooling unit with ice water circulation that kept the temperature in the chamber headspace close to the ambient. Data on CO_2 concentration, air temperature inside and outside the chamber (107 Thermistor Probe C/W, Campbell Scientific, UK) and PAR (SKP215, Skye Instruments, UK) was collected to a data logger (CR850, Campbell Scientific) at 2 s intervals during 2 min measurements.

Net ecosystem CO_2 exchange (NEE) measurements were done in ambient and reduced light conditions (~ 50 % PAR), created by shadowing the chamber with a net. For measuring ecosystem respiration (ER) the chamber was darkened with an aluminum lid. Each microsite had 3 replicate soil collars (depth 15 cm) that served as permanent measurement plots. At the willow site additional collars (height 60 cm) were used during the CO_2 flux measurements.

Carbon dioxide fluxes were calculated from the increase in CO_2 concentration in the chamber headspace using an exponential non-linear model by Kutzbach et al. (2007a) in MATLAB (R2008a) program. Residual standard deviation of the regression > 1.5 ppm was used as a filtering criterion, based on which 2 % of the flux data were rejected. Gross photosynthesis (GP) was calculated as a difference between consecutive NEE and ER measurements.

BGD
9, 9945–9991, 2012

2.3.2 Modeling gross photosynthesis and ecosystem respiration

The two components of net CO_2 flux, GP and ER, were modeled over the measuring period based on their dependence on environmental parameters using nonlinear regression in SPSS 14.0 statistical software (Table 3). Ecosystem respiration was modeled individually for each chamber plot, while parameterization of the more complex GP models was done at the microsite level. Data was split by years, and for GP modeling growing season 2008 was further divided into early and late season. The GP models included a Michaelis-Menten type equation for the light response, a Gaussian or linear temperature term and a linear LAI term. The LAI data from 2008 was used also for 2007, which was justified by the good model fit in 2007. For surfaces without any vascular plants ("Bare peat") a soil moisture term was used instead of the LAI term. Ecosystem respiration was modelled using an Arrhenius type temperature dependence (Lloyd and Taylor, 1994). Anomalously high respiration peaks at soil freezing and thawing (2 % of all data) were removed before the modeling (Supplement Fig. S1).

2.3.3 Carbon dioxide fluxes during snow period

During the snow period CO_2 fluxes were measured with a snow-gradient method as described by Marushchak et al. (2011). Fluxes were determined in January–June 2008 total 2–5 times per plot depending the timing of the snow melt. The samples were stored in glass vials max. three months before analysis on a gas chromatograph (HP 5890 series II, Hewlett-Packard, USA) with a thermal conductivity (TC) detector for CO_2 (Nykänen et al., 1995). A leakage test with a gas standard (2500 ppm) showed that the reduction of CO_2 concentration in the sample vials over two months was ≤ 3 % (data not shown).

BGD
9, 9945–9991, 2012

2.3.4 Carbon dioxide fluxes from lakes

Emission of CO_2 by diffusion and ebullition pathways was studied in three thermokarst lakes from July to August 2007 (11 samplings) and from June to October 2008 (19 samplings). The determination of CO_2 concentrations in the surface water and flux calculation using the thin boundary layer model followed Repo et al. (2007). Surface water samples were collected during daytime (08:00 a.m.–19:00 p.m.). Linearly interpolated daily CO_2 concentrations and hourly wind speed (measured at 2 m, normalized to 10 m using a logarithmic wind profile) were used to calculate hourly flux rates. Ebullitive CO_2 flux was monitored with permanently installed submerged funnel gas collectors (Repo et al., 2007). Each lake had 6–7 replicate gas collectors (Ø 0.35 m). Gas samples were stored and analyzed as described above.

2.4 Carbon dioxide exchange at landscape scale

2.4.1 Eddy covariance setup

Landscape-scale NEE was measured in May–October 2008 (days 139–280) at a frequency of 10 Hz using the micrometeorological EC method (Aubinet et al., 2000; Baldocchi, 2003). The system was set up with an R3 ultrasonic anemometer (Gill Instruments, UK) and an LI-7500 open-path CO_2/H_2O IRGA (LI-COR) mounted at 3.95 m height. The power was supplied by a fuel generator placed 40 m east-south east (110°) of the mast.

2.4.2 Data processing

The raw data were processed using the Alteddy software (version 3.5, University of Wageningen, The Netherlands, http://www.climatexchange.nl/projects/alteddy/), which is based on EUROFLUX methodology (Aubinet et al., 2000). The means and variances of turbulent CO_2 fluxes (= NEE) were calculated in half-hour time-steps.

BGD
9, 9945–9991, 2012

The open-path gas analyzer bears the disadvantage of self heating of the instrument surface which may result in overestimation of the CO_2 uptake especially under cold conditions (e.g., Goulden et al., 2006; Ono et al., 2008). To account for this effect we applied the correction proposed by Burba et al. (2008). The quality of the data was assessed using quality flags according to Foken and Leclerc (2004), and only data with quality flags between 1 and 6 was included to the final dataset. Furthermore, data were rejected when measured during rain and fog events, when the wind was from the direction of the generator (90 to 130°) and when friction velocity (u^*) was $< 0.1\,m\,s^{-1}$. Out of the 6835 measured half-hourly NEE fluxes 50 % passed these criteria.

Subsequent gaps in the time-series were filled using an online tool (http://www.bgc-jena.mpg.de/bgc-mdi/html/eddyproc/) based on the algorithms by Falge et al. (2001) and Reichstein et al. (2005). A nighttime gap from 25 August to 6 October 2008 (days 238–280) was filled using a regression function based on soil temperature (Lloyd and Taylor, 1994; see below). During this period, 70 % of the nighttime values had to be discarded due to rain events, dew formation or low turbulence conditions, which made the use of the online tool unfeasible.

2.4.3 Night time fluxes and flux partitioning

Measured NEE was partitioned into its components, GP and ER, by modeling ER based on its temperature response. For this purpose, we used the night time NEE (PAR $< 50\,\mu mol\,m^{-2}\,s^{-1}$) that is equal to ER. Only flux data with a quality flag 1–3 were used. The regression was performed on nightly average fluxes and soil temperatures by fitting data into an Arrhenius type function (Lloyd and Taylor, 1994):

$$R_{ECO} = R_{10} \cdot \exp(308.6 \cdot (1/56) - (1/(T_s + 46))), \quad (1)$$

where R_{10} is the ER at 10 °C and T_s is the soil temperature at 5 cm in °C. GP was calculated as a difference between NEE and ER. The temperature response of ER is shown in Supplement Fig. S2.

BGD
9, 9945–9991, 2012

2.4.4 Footprint analysis

The flux measured by the EC technique originates from a large number of ground level point sources located on various LCTs. The contribution of each point within source area, so called footprint, to the EC flux was calculated by spatial integration of the source weight function. The footprint analysis was performed in MATLAB R2009a using a footprint model originally developed in 2-D by Gash (1986) and Schuepp et al. (1990) and expanded for use in 3-D by Soegaard et al. (2003). The contribution of each LCT to the footprint area was calculated by the model for each 30 min observation interval. For this purpose, the spatial source weights were determined within a 2.5 km radius around the mast for each 2.4 m × 2.4 m grid cell of the QuickBird image. By superimposing these grid source weights upon the land cover map (see below), the contribution of each LCT to the recorded flux could be estimated.

2.5 Up-scaling of the fluxes using remote sensing data

2.5.1 Land-cover classification

The LCC, used for scaling up the CO_2 balance, was based on a QuickBird satellite image covering 98.6 km^2 around flux measurement site, acquired on 6 July 2007 (QuickBird© 2007, DigitalGlobe; Distributed by Eurimage/Pöyry) (Fig. 1a). Four channels were used in the classification procedure (blue, green, red and infrared (NIR); pixel size 2.4 m). Classifications were produced using a multiple level segmentation in the Definiens Professional 5.0 software. Vegetation descriptions made at 150 transects points and additional field notes and photographs were used as ground-truthing data. The classification was tested using vegetation descriptions from 130 randomly selected field points. The classification is described in more detail by Hugelius et al. (2011).

From the total of 13 LCTs 8 were studied with plot scale techniques. Five LCTs corresponded directly to microsites studied, while some incorporated more than one microsite type (Table 2). The relative contribution of different microsites within these

BGD
9, 9945–9991, 2012

LCTs was estimated from photographs taken at transect points around the EC mast. The chamber fluxes of different LCTs were weighed by their relative area contributions in order to obtain CO_2 balance over the study area. For rivers, we used the CO_2 emission of 33 g C m^{-2} during open water period (100 days), measured in the same region by Heikkinen et al. (2004). A zero CO_2 balance was assumed for forest stands, sand and impacted tundra.

2.5.2 Leaf area index mapping

LAI map was developed using the same QuickBird satellite image as for LCC. It was based on a regression model, where mean LAI values for growing period measured in the field (Fig. 1b) were predicted by NDVI (Normalized Difference Vegetation Index: (NIR – red)/(NIR + red)) and individual channel reflectance values. Mean values from 5-m radius around the LAI measurement points were calculated from the QuickBird data in order to eliminate spatial inaccuracies caused by GPS device. Square root transformation was used for the LAI values. NDVI was the best single explanatory variable to explain LAI (30 % of variation), and by adding channels 1 (blue) and 2 (green) the explanatory power was increased to 36 %. The residuals of the model were normally distributed. The rather large unexplained variation can be explained by the fact that the LAI measurements were made at single points and vegetation cover around them was not uniform enough to perfectly match the satellite data. When the model was applied to the whole QuickBird image, predicted negative LAI-values were re-classified as 0. Mean LAI for the terrestrial surfaces was calculated by subtracting the waterbodies from the LAI of the whole region. Dependence between cumulative CO_2 fluxes and LAI, observed for terrestrial microsites, was used to calculate the regional CO_2 balance.

2.6 Uncertainty estimates for the CO_2 fluxes

Uncertainty of the CO_2 balance from area-integrated plot scale measurements was estimated by weighing the standard deviations (SDs) of hourly microsite fluxes with

BGD
9, 9945–9991, 2012

corresponding area contributions, and summing up these area-weighed SDs over time. For EC fluxes, the gap filling procedure was considered as the main uncertainty factor due to the high percent of gap filled values (51 %). Artificial gaps were added to the dataset and subsequently modeled by usual gap filling procedure describe above. These artificial gap filled fluxes and the original fluxes showed a good agreement with a R^2 of 0.85 and RSME of 1.3 µmol m^{-2} s^{-1}. The average daily difference between the artificial gap filled and original measured fluxes was considered as the uncertainty of the EC flux.

3 Results

3.1 Meteorology

The seasonal course of air temperature and precipitation from July 2007 to October 2008 are shown in Fig. 2. Air temperatures were above the long term means in December, January and in July, which was hot especially in 2007 (Table 1). The precipitation during the snow-free period 2007–2008 was mostly equal to the long term mean. The length of the thermic growing season, defined as a period when the daily mean air temperature is permanently above +5 °C, was 80 days in 2007 and 79 days in 2008. The permanent snow cover lasted from mid October to mid May–early June.

3.2 LAI map

The distribution of LAI values predicted by the regression model based on spectral satellite data is realistic when assessed in relation to the LCC (Fig. 1a–b). Overall mean LAI for the region was 0.98 (max 5.36). The proportion of zero LAI values (1.8 %) matched very well to the coverage of water and non-vegetated soils in the LCC (1.6 %). There was a strong correlation between the LAI values measured at the chamber plots and those derived from the LAI map for different land-cover classes ($p < 0.01$; Fig. 3). The only LCTs deviating from 1 : 1 line were Fen and *Betula nana* tundra heath.

BGD
9, 9945–9991, 2012

3.3 Spatial variability in CO_2 exchange

Figure 4 shows the raw chamber data that was used for building the experimental models to predict CO_2 fluxes at the terrestrial microsites (Table 3). We follow a sign convention where C loss from the ecosystem is defined as positive and C uptake as negative values. The models were able to explain 86 and 74 % of the observed overall variability in the measured GP and ER fluxes (Fig. 5). Details of the models are presented in Supplement Tables S1 and S2.

The spatial variability in soil conditions and vascular plant cover (Table 4) resulted in large differences in CO_2 fluxes across the landscape (Figs. 6–7). The growing season ER of terrestrial microsites varied from 64 to 226 g C m^{-2}, GP from −31 to −518 g C m^{-2} and NEE from −292 to 48 g C m^{-2}. The annual CO_2 balance ranged from −251 to 84 g C m^{-2}. A general trend of increasing C uptake with increasing wetness (upland tundra < dry peatlands < wetlands) was observed for the three main LCTs (Fig. 6), and wetlands also had the highest ER of the main LCTs. The mean LAI was an excellent predictor of the growing season GP and NEE, and even of the ER (Fig. 8). Moreover, the predictive power of LAI was good also for annual CO_2 fluxes (data not shown). Microsites with LAI < 0.3 (Dry shrub tundra heath, Dry lichen tundra heath, Bare peat, *Eriophorum* dominated fen) had the lowest GP and were net sources of C to the atmosphere on an annual basis. All the other microsites showed annual net uptake of C.

The thermokarst lakes studied were supersaturated with CO_2 and, thus, atmospheric sources of this gas during the whole open water period (Fig. 9). The annual emissions of CO_2 from the three lakes ranged from 13 to 82 g C m^{-2}, averaging 43 ± 35 g C m^{-2}. Diffusion was the main pathway of CO_2 release, the importance of ebullition being negligible. The maximum CO_2 release from lakes, ∼1.0 g C m^{-2} d^{-1}, was moderate compared to the ER in terrestrial microsites.

BGD
9, 9945–9991, 2012

3.4 Temporal variability CO_2 exchange

3.4.1 Seasonal variations

A distinct seasonal pattern in the diurnal course of NEE was revealed when the half-hourly EC fluxes were averaged according to the time of the day over 14-day periods (Fig. 10). Until 15 June the CO_2 exchange all the average half-hourly net fluxes were directed to the atmosphere. During 16–30 June, a clear diurnal pattern was established. The maximum amplitude of the diurnal variation was observed during the second half of July when both nighttime respiration and daytime net uptake reached the maximum values (4 µmol m^{-2} s^{-1} and −8 µmol m^{-2} s^{-1}, respectively). From August onwards the fluxes decreased until the end of the measurement period.

Modeled plot scale fluxes showed an initiation of the summer uptake period on day 170–178 (Fig. 6), while first day with daily net C uptake observed by EC was day 174. In autumn, the EC measurements indicated a shift to a daily source already on day 240, area integrated plot scale measurements only on day 258 (Fig. 4). The seasonal amplitude of NEE was higher for EC fluxes than for the area integrated plot scale measurements, i.e., EC showed higher net uptake rates during mid-summer and higher net CO_2 release during early and late season.

Based on the plot scale measurements the non-growing season ER comprised 25–45 % of the annual ER. The measured values of winter-time respiration were 0–0.24 µmol m^{-2} s^{-1} in January and 0–0.22 µmol m^{-2} s^{-1} in March. The areal integrated ER for the EC footprint based on modeling results was within the range of the measured respiration rates, 0.13 and 0.11 µmol m^{-2} s^{-1} for January and March, respectively. We observed a clear peak in ER at top-soil (2 cm) temperatures ∼0°C in upland tundra and dry peatlands, but not in wetlands (Supplement Fig. S1). The peak was more pronounced in the spring than in the fall.

BGD
9, 9945–9991, 2012

3.4.2 Interannual variations

Interannual comparison is limited to July and August, the only months with intensive chamber measurements during the both study years (Fig. 11). Upland microsites (n = 12) had 25 % higher ER in July–August 2007 than in 2008 (Wilcoxon Signed Ranks Test; $p < 0.05$). 75 % of the cumulative difference in ER occurred in July that had higher air and top soil temperatures in 2007 than in 2008. As a result of the higher respiration, the net C sink on upland was by 50 % lower in 2007, while the GP was similar during both years. No interannual differences were observed in the peak-season GP, NEE or ER on wetlands and dry peatlands. Also the CO_2 emissions from thermokarst lakes were of similar magnitude in growing seasons 2007 and 2008 (20 ± 18 g C m^{-2} and 29 ± 22 g C m^{-2}, respectively).

3.5 Comparison of CO_2 balances by the two measuring techniques in landscape scale

The EC and area integrated plot scale measurements resulted in similar CO_2 sink strength for the EC footprint during growing season 2008 (-81 ± 37 g C m^{-2} vs. -105 ± 27 to -79 ± 35 g C m^{-2}, respectively; Table 5). Outside the growing season EC showed a higher source than the plot scale measurements (up-scaled with LCC), the mean difference being 0.44 g C m^{-2} d^{-1} in the early season and 0.82 g C m^{-2} d^{-1} in the late season. Still, the CO_2 balances based on the two methods were within the error range of each other for the whole EC measuring period of 141 days. Up-scaling with LAI map resulted in somewhat stronger sink than up-scaling with LCC, but the difference was not significant.

The partitioning approach used for the EC fluxes (Fig. 12) allows the comparison of the two CO_2 flux components, ER and GP, between the two methods. Although the EC and area-integrated chambers resulted in similar cumulative NEE for the growing season, the plot scale measurements showed lower fluxes to both directions. Cumulative ER and GP for the growing season from EC were 226 and

BGD
9, 9945–9991, 2012

$-305\,g\,C\,m^{-2}$ ($-ER/GP = 0.74$) and from plot scale measurements 111 to 130 and -233 to $-188\,g\,C\,m^{-2}$ ($-ER/GP = 0.56$–0.59).

3.6 Seasonal and annual CO_2 balance for the study region

After verifying the plot scale fluxes by comparing them with the EC results in the landscape scale, we scaled them up to the whole QuickBird area of 98.6 km^2. The regional CO_2 balance during the growing season 2008 was -127 ± 30 to $-94 \pm 37\,g\,C\,m^{-2}$ based on the two independent up-scaling approaches. The annual CO_2 balance (NEE) for the study region was -79 ± 22 to $-41 \pm 57\,g\,C\,m^{-2}$, consisting of ER of 197 ± 35 to $212 \pm 50\,g\,C\,m^{-2}$ and GP of -294 ± 58 to $-238 \pm 39\,g\,C\,m^{-2}$. 33–39 % of the annual ER and 8–10 % of the annual GP occurred outside the growing season. The study region as a whole was a 16–21 % stronger CO_2 sink than the EC footprint area, which corresponds to difference in LAI between the two scales (0.98 vs. 0.83). The EC footprint had, e.g., more tundra bog and lakes and less willows than the whole region (Supplement Fig. S3).

4 Discussion

4.1 Plot scale CO_2 fluxes

Despite the heterogeneity of the studied landscape, a clear trend was found to explain the spatial variability in CO_2 exchange. Vascular LAI explained ~ 90 % of the variability in the growing season GP and NEE across the studied microsites, and even for ER its explanatory power was 67 %. Given that the CO_2 fluxes were modeled independently for each microsite, this was a true dependence, not a modeling artifact. Since non-destructive LAI measurements with a plant canopy analyzer are fast and easy and can be related to remote sensing data, the strong relationship between LAI and CO_2 fluxes is very promising from the up-scaling point of view. Also in earlier studies on

BGD
9, 9945–9991, 2012

tundra and peatland ecosystems LAI has explained well the spatial variability in GP (Lund et al., 2010) or both GP and ER (Soegaard et al., 2000; McFadden et al., 2003; Humphreys et al., 2006). Positive correlation between ER and LAI may be explained by dominance of autotrophic respiration over microbial decomposition of soil organic matter (heterotrophic respiration), or tight link between these two respiration components through, e.g., rhizomicrobial respiration (Hutsch et al., 2002).

We did not observe significant differences in GP between the study years at any of the land cover types. However, the peak summer ER was higher and net CO_2 sink smaller on uplands in 2007 that was warmer of the two years. There was no similar increase in ER at the peatland sites, most probably due to wetter soil conditions that were limiting soil respiration over temperature. Similarly, Heikkinen et al. (2004) measured higher ER from non-water logged soils in the same region during the warmer and drier of the two study years. Also in the same region, Zamolodchikov et al. (2000) observed in shrub tundra communities (on upland tundra) a switch in net C flux from sink to source when canopy temperature rose above +14 °C.

The wintertime ER data obtained by plot scale measurements are within the range reported earlier for similar ecosystems. Our mean CO_2 efflux in January-March was similar to winter time respiration reported for northern peatlands and tundra (e.g., Oechel et al., 1997; Elberling, 2007; Lund et al., 2010). Also the area-integrated estimate for non-growing season ER ($77\,g\,C\,m^{-2}$) falls within the wide range of previous estimates on cumulative winter-time ER from 1 to $104\,g\,C\,m^{-2}$ (Zimov et al., 1996; Heikkinen et al., 2002; Oechel et al., 1997, 2000; Elberling, 2007; Kutzbach et al., 2007b; Vogel et al., 2009).

4.2 Differences in landscape scale CO_2 fluxes between the two measuring techniques

The two methods used to measure CO_2 exchange resulted in very similar CO_2 balances for the growing season. However, there were differences between EC and area-integrated plot scale measurements (i) in the timing of onset and conclusion of the net

BGD
9, 9945–9991, 2012

uptake period, and (ii) in the magnitude of the two components of CO_2 flux, ER and GP. Due to these differences, the chambers showed still a significant CO_2 sink for the whole EC measuring period from May to October, while the CO_2 balance from EC was negative, but did not differ significantly from zero.

The correct timing and length of the summer uptake period is not easy to catch when the seasonal CO_2 balance is estimated based on modeled chamber data. More frequent measurements of LAI and fluxes during spring and autumn would have helped to determine the start and end of net uptake period more accurately. However, the differences in the timing of the summer uptake period were not a major reason for the discrepancy between the two methods in the cumulative CO_2 flux for the EC measuring period.

The area-integrated chambers showed lower amplitude of the seasonal NEE cycle, and partitioning of the EC fluxes into ER and GP components revealed that the chamber based CO_2 fluxes were lower to both directions. Indeed, there are problems related with the closed chamber technique that may causes underestimation of the gas flux, such as reduction of the concentration gradient between the soil and the atmosphere (Kutzbach et al., 2007a) or underestimation of the effective chamber volume when the air-filled soil pore space is not accounted for Rayment (2000). We took care of all necessary precautions to avoid chamber bias: the incubation time was kept short, and fluxes were calculated using non-linear regression. At our dry microsites, underestimation of effective chamber volume may have caused some bias in the fluxes. Also, it must be kept in mind here that the chamber fluxes used for the areal integration were modelling results whereas NEE dynamics from EC were obtained by direct measurements. A feature of all models is that they are dominated by the data in the middle of the data range and tend to filter out the extremes.

A known problem of the open path EC gas analyzer is the overestimation of the C uptake during the cold season due to the heating of the sensor head (e.g., Goulden et al., 2006; Ono et al., 2008). Also in this study a spring uptake up to 0.5 g C m^{-2} d^{-1} was observed while the landscape was still covered by snow, and the correction suggested

BGD
9, 9945–9991, 2012

by Burba et al. (2008) was applied on the data. Since the sensible heat flux in the optical path was not directly measured, the correction was based on the measured air temperature (Burba et al., 2008; method 4). This may have caused overcorrection of the fluxes (Wohlfahrt et al., 2008; Bowling et al., 2010).

Biased selection of chamber plots (see Fox et al., 2008) or a failure to estimate correctly the coverage of different LCTs would also lead to biased flux estimates, particularly when the high spatial variability in CO_2 fluxes is so high. In our study, we found a good match in LAI values between the chamber plots and the corresponding LCTs as a whole, showing that the chamber plots were well representative. Further, we can be sure that our QuickBird based LCC described the patchy tundra vegetation better than previously used Landsat image classifications with 30 m pixel size (Soegaard et al., 2000; Heikkinen et al., 2004). While the size of one Landsat image pixel is 900 m^2 the mean patch size in this study was 816 m^2. The mean patch size of fens, for example, was only 260 m^2. With the high-resolution LCC we could accurately represent this small scale variability in vegetation.

To conclude, we cannot fully explain the observed differences in CO_2 fluxes between the two measuring techniques. However, the growing season CO_2 balances from the two methods were strikingly similar giving high confidence in the reported CO_2 sink strength during summer.

4.3 Regional CO_2 balance

The regional CO_2 balance of the tundra area of 98.6 km^2 was obtained by up-scaling the plot scale measurements using independent approaches. From October 2007 to October 2008 the studied tundra acted as a CO_2 sink of −79 to −41 g C m^{-2} yr^{-1}. The gross CO_2 fluxes (GP = −294 to −238 g C m^{-2} yr^{-1} and ER = 197 to 212 g C m^{-2} yr^{-1}) where relatively large compared with the earlier studies summarized in Table 6. This could be due to the milder climatic conditions prevailing in the southern East European tundra compared with high arctic and more continental sites (see Zamolodchikov and Karelin, 2001). However, this is a simplistic explanation for the observed since large

BGD
9, 9945–9991, 2012

site-specific differences exist even within climatic zones. For example, lowlands with wet soils typically have higher C accumulation rates than upland tundra in the same region (e.g., Vourlitis et al., 2000; Kwon et al., 2006).

The dependence of CO_2 on vascular LAI, discussed above, would provide a more generic explanation for the variability in CO_2 budgets. If we assume that this dependence holds true also across the different study sites, the relatively high gross CO_2 fluxes at the Seida site could be related to high aboveground biomass compared with the reference studies. It must be noted here that the C budgets of northern ecosystems also show very large interannual variability, driven by variability in weather conditions (e.g., Aurela et al., 2004; Groendahl et al., 2007; Lafleur and Humphreys, 2008; Lund et al., 2010, 2012). The two study years were warmer than the long term mean, and particularly high temperatures were measured in July during the intensive growth period (3–5 °C higher than the long term mean). This might have enhanced the both flux components, GP and ER.

4.4 Effects of climate change on regional CO_2 balance

The net effect of climate change on the C balance will be a sum of various changes happening at different land cover types. The willow stands, currently responsible for 27 % of the growing season net CO_2 uptake, may become even more important with future warming based on the trend of increased willow growth observed during the last decades in the region (Forbes et al., 2010). Studies from Northern Alaska show that also deciduous shrubs dominant in upland tundra will benefit from warmer temperatures (Tape et al., 2006). According to the dependence observed between LAI and NEE, better growth of vascular plants would mean increased net C sink to the studied tundra ecosystem. However, multiannual flux studies have shown that in some tundra ecosystems vegetation communities are well adapted to the present temperatures, and warmer summer temperatures may even lead to lower net C sink (Parmentier et al., 2011; Lund et al., 2012). Further, in the long run increase of C uptake by plant growth may be counterbalanced by the enhanced decomposition of SOC because of

BGD
9, 9945–9991, 2012

warmer soils and deepening of the active soil layer due to permafrost thaw (Schuur et al., 2009; Dorrepaal et al., 2009). Permafrost thawing may increase the C release particularly at peat plateaus with shallow seasonal thaw depth, if a thicker soil layer will become available for microbial decomposition. In upland tundra, the seasonal thaw is already rather deep but still the increased air and soil temperatures might threaten the CO_2 sink character by increasing respiration over carbon uptake (this study; Heikkinen et al., 2004; Zamolodchikov et al., 2000; Lund et al., 2012).

Besides the effect of climate change on area-specific CO_2 balance of different land cover types, changes are expected also in their relative coverage. For example, the coverage of fen type peatlands will likely increase at the expense of peat plateaus (e.g., Johansson et al., 2006), which would increase the C uptake at regional scale because of the higher CO_2 sink character of fens. Due to the large differences in CO_2 balance between different tundra surfaces in the study region, landscape reorganization will have a strong influence on regional CO_2 balance.

Appendix A

Abbreviations

ER	Ecosystem respiration
GP	Gross photosynthesis
LAI	Leaf area index
LCC	Land cover classification
LCT	Land cover type
NEE	Net ecosystem CO_2 exchange

BGD
9, 9945–9991, 2012

Supplementary material related to this article is available online at: http://www.biogeosciences-discuss.net/9/9945/2012/bgd-9-9945-2012-supplement.pdf.

Acknowledgements. We want to thank the following people for their contribution in the field work and data analysis: Petr Ievlev, Simo Jokinen, Saara Lind, Igor Marushchak, Aleksander Novakovsky, Irina Samarina, Vladimir Shchanov and Tatiana Trubnikova (plot scale measurements), Anders Anker Bjoerk, Tobias Diaoli, Thomas Grelle, Mathias Herbst, Rasmus Jensen, Theis Schmidt Knudsen, Daniel Grube Pedersen and Jens Bjerg Bertelsen Sand (EC measurements), and Malin Ek, Tiina Ronkainen and Sanna Susiluoto (vegetation and remote sensing data). This study belongs to the EU 6th Framework Programme project CARBO-North (contract number 036993; www.carbonorth.net). M. E. Marushchak received personal funding from the Finnish Graduate School of Forest Sciences. I. Kiepe received funding by the Danish Council for Independent Research |Natural Sciences (FNU) (Reference number: 645-06-0493).

References

Aubinet, M., Grelle, A., Ibrom, A., Rannik, U., Moncrieff, J., Foken, T., Kowalski, A. S., Martin, P., Berbigier, P., Bernhofer, C., Clement, R., Elbers, J., Granier, A., Grunwald, T., Morgenstern K., Pilegaard, K., Rebmann, C., Snijders, W., Valentini, R., and Vesala, T.: Estimates of the annual net carbon and water exchange of forests: The EUROFLUX methodology, Adv. Ecol. Res., 30, 113–175, doi:10.1016/S0065-2504(08)60018-5, 2000.

Aurela, M., Laurila, T., and Tuovinen, J.: The timing of snow melt controls the annual CO_2 balance in a subarctic fen, Geophys. Res. Lett., 31, L16119, doi:10.1029/2004GL020315, 2004.

Bäckstrand, K., Crill, P. M., Jackowicz-Korczyński, M., Mastepanov, M., Christensen, T. R., and Bastviken, D.: Annual carbon gas budget for a subarctic peatland, Northern Sweden, Biogeosciences, 7, 95–108, doi:10.5194/bg-7-95-2010, 2010.

Baldocchi, D.: Assessing the eddy covariance technique for evaluating carbon dioxide exchange rates of ecosystems: past, present and future, Glob. Change Biol., 9, 479–492, doi:10.1046/j.1365-2486.2003.00629.x, 2003.

BGD
9, 9945–9991, 2012

Bazilevich, N. I.: Biological productivity of ecosystems of Northern Eurasia. Nauka, Moscow, 293 pp., 1993.
Bowling, D. R., Bethers-Marchetti, S., Lunch, C. K., Grote, E. E., and Belnap, J.: Carbon, water, and energy fluxes in a semiarid cold desert grassland during and following multiyear drought, J. Geophys. Res.-Biogeo., 115, G04026, doi:10.1029/2010JG001322, 2010.
Burba, G. G., McDermitt, D. K., Grelle, A., Anderson, D. J., and Xu, L.: Addressing the influence of instrument surface heat exchange on the measurements of CO_2 flux from open-path gas analyzers, Glob. Change Biol., 14, 1854–1876, doi:10.1111/j.1365-2486.2008.01606.x, 2008.
Christensen, T. R., Friborg, T., Sommerkorn, M., Kaplan, J., Illeris, L., Soegaard, H., Nordstroem, C., and Jonasson, S.: Trace gas exchange in a high-arctic valley 1. Variations in CO_2 and CH_4 flux between tundra vegetation types, Global Biogeochem. Cy., 14, 701–713, doi:10.1029/1999GB001134, 2000.
Corradi, C., Kolle, O., Walter, K., Zimov, S. A., and Schulze, E.-D.: Carbon dioxide and methane exchange of a north-east Siberian tussock tundra, Glob. Change Biol., 11, 1910–1925, doi:10.1111/j.1365-2486.2005.01023.x, 2005.
Dorrepaal, E., Toet, S., van Logtestijn, R. S. P., Swart, E., van de Weg, M. J., Callaghan, T. V., and Aerts, R.: Carbon respiration from subsurface peat accelerated by climate warming in the subarctic, Nature, 460, 616–619, doi:10.1038/nature08216, 2009.
Elberling, B.: Annual soil CO_2 effluxes in the High Arctic: The role of snow thickness and vegetation type, Soil Biol. Biochem., 39, 646–654, doi:10.1016/j.soilbio.2006.09.017, 2007.
Falge, E., Baldocchi, D., Olson, R., Anthoni, P., and Aubinet, M.: Gap filling strategies for defensible annual sums of net ecosystem exchange, Agr. Forest Meteorol., 107, 43–69, doi:10.1016/S0168-1923(00)00225-2, 2001.
Foken, T., Göckede, M., Mauder, M., Mahrt, L., Amiro, B., and Munger, W.: Post-field data quality control, in: Handbook of Micrometeorology, edited by: Lee, X., Massman, W., and Law, B., Springer, Berlin, Heidelberg, New York, 181–208, 2004.
Forbes, B. C., Macias Fauria, M., and Zetterberg, P.: Russian Arctic warming and "greening" are closely tracked by tundra shrub willows, Glob. Change Biol., 16, 1542–1554, doi:10.1111/j.1365-2486.2009.02047.x, 2010.
Fox, A. M., Huntley, B., Lloyd, C. R., Williams, M., and Baxter, R.: Net ecosystem exchange over heterogeneous Arctic tundra: Scaling between chamber and eddy covariance measurements, Global Biogeochem. Cy., 22, GB2027, doi:10.1029/2007GB003027, 2008.

BGD
9, 9945–9991, 2012

Fuchs, H., Magdon, P., Kleinn, C., and Flessa, H.: Estimating aboveground carbon in a catchment of the Siberian forest tundra: Combining satellite imagery and field inventory, Remote Sens. Environ., 113, 518–531, doi:10.1016/j.rse.2008.07.017, 2009.

Gash, J. H. C.: A note on estimating the effect of a limited fetch on micrometeorological evaporation measurements, Bound.-Lay. Meteorol., 35, 409–413, 1986.

Goulden, M. L., Winston, G. C., McMillan, A. M. S., Litvak, M. E., Read, E. L., Rocha, A. V., and Elliot, J. R.: An eddy covariance mesonet to measure the effect of forest age on land-atmosphere exchange, Glob. Change Biol., 12, 2146–2162, doi:10.1111/j.1365-2486.2006.01251.x, 2006.

Groendahl, L., Friborg, T., and Soegaard, H.: Temperature and snow-melt controls on interannual variability in carbon exchange in the high Arctic, Theor. Appl. Climatol., 88, 111–125, doi:10.1007/s00704-005-0228-y, 2007.

Harazono, Y., Mano, M., Miyata, A., Zulueta, R., and Oechel, W.: Inter-annual carbon dioxide uptake of a wet sedge tundra ecosystem in the Arctic, Tellus B, 55, 215–231, doi:10.1034/j.1600-0889.2003.00012.x, 2003.

Heikkinen, J. E. P., Elsakov, V., and Martikainen, P. J.: Carbon dioxide and methane dynamics and annual carbon balance in tundra wetland in NE Europe, Russia, Global Biogeochem. Cy., 16, 1115, doi:10.1029/2002GB001930, 2002.

Heikkinen, J. E. P., Virtanen, T., Huttunen, J. T., Elsakov, V., and Martikainen, P. J.: Carbon balance in East European tundra, Global Biogeochem. Cy., 18, GB1023, doi:10.1029/2003GB002054, 2004.

Hugelius, G., Virtanen, T., Kaverin, D., Pastukhov, A., Rivkin, F., Marchenko, S., Romanovsky, V., and Kuhry, P.: High-resolution mapping of ecosystem carbon storage and potential effects of permafrost thaw in periglacial terrain, European Russian Arctic, J. Geophys. Res.-Biogeo., 116, G03024, doi:10.1029/2010JG001606, 2011.

Humphreys, E. R. and Lafleur, P. M.: Does earlier snowmelt lead to greater CO_2 sequestration in two low Arctic tundra ecosystems?, Geophys. Res. Lett., 38, L09703, doi:10.1029/2011GL047339, 2011.

Hutsch, B., Augustin, J., and Merbach, W.: Plant rhizodeposition – an important source for carbon turnover in soils, Z. Pflanzenernähr. Bodenk., 165, 397–407, doi:10.1002/1522-2624(200208)165:4<397::AID-JPLN397>3.0.CO;2-C, 2002.

Johansson, T., Malmer, N., Crill, P. M., Friborg, T., Akerman, J. H., Mastepanov, M., and Christensen, T. R.: Decadal vegetation changes in a northern peatland, greenhouse gas

BGD
9, 9945–9991, 2012

fluxes and net radiative forcing, Glob. Change Biol., 12, 2352–2369, doi:10.1111/j.1365-2486.2006.01267.x, 2006.
Kattsov, V. M., Källén, E., Cattle, H., Christensen, J., Drange, H., Hanssen-Bauer, I., Jóhannesen, T., Karol, I., Räisänen, J., Svensson, G., and Vavulin, S.: Future climate change: Modeling and scenarios for the Arctic, in: Arctic Climate Impact Assessment, edited by: Symon, C., Arris, L., and Heal, B., Cambridge University Press, New York, 99–150, 2005.
Kutzbach, L., Schneider, J., Sachs, T., Giebels, M., Nykänen, H., Shurpali, N. J., Martikainen, P. J., Alm, J., and Wilmking, M.: CO_2 flux determination by closed-chamber methods can be seriously biased by inappropriate application of linear regression, Biogeosciences, 4, 1005–1025, doi:10.5194/bg-4-1005-2007, 2007a.
Kutzbach, L., Wille, C., and Pfeiffer, E.-M.: The exchange of carbon dioxide between wet arctic tundra and the atmosphere at the Lena River Delta, Northern Siberia, Biogeosciences, 4, 869–890, doi:10.5194/bg-4-869-2007, 2007b.
Kwon, H., Oechel, W. C., Zulueta, R. C., and Hastings, S. J.: Effects of climate variability on carbon sequestration among adjacent wet sedge tundra and moist tussock tundra ecosystems, J. Geophys. Res.-Biogeo., 111, G03014, doi:10.1029/2005JG000036, 2006.
Lafleur, P. M. and Humphreys, E. R.: Spring warming and carbon dioxide exchange over low Arctic tundra in central Canada, Glob. Change Biol., 14, 740–756, doi:10.1111/j.1365-2486.2007.01529.x, 2008.
Laidler, G. J. and Treitz, P.: Biophysical remote sensing of arctic environments, Prog. Phys. Geogr., 27, 44–68, doi:10.1191/0309133303pp358ra, 2003.
Lloyd, C. R.: On the physical controls of the carbon dioxide balance at a high Arctic site in Svalbard, Theor. Appl. Climatol., 70, 167–182, doi:10.1007/s007040170013, 2001.
Lloyd, J. and Taylor, J. A.: On the temperature-dependence of soil respiration, Funct. Ecol., 8, 315–323, 1994.
Lund, M., Falk, J. M., Friborg, T., Mbufong, H. N., Sigsgaard, C., Soegaard, H., and Tamstorf, M. P.: Variability in exchange of CO_2 across 12 northern peatland and tundra sites, Glob. Change Biol., 16, 2436–2448, doi:10.1111/j.1365-2486.2009.02104.x, 2010.
Lund, M., Falk, J. M., Friborg, T., Mbufong, H. N., Sigsgaard, C., Soegaard, H., and Tamstorf, M. P.: Trends in CO_2 exchange in a high Arctic tundra heath, 2000–2010, J. Geophys. Res., 117, G02001, doi:10.1029/2011JG001901, 2012.

BGD
9, 9945–9991, 2012

Marushchak, M. E., Pitkämäki, A., Koponen, H., Biasi, C., Seppälä, M., and Martikainen, P. J.: Hot spots for nitrous oxide emissions found in different types of permafrost peatlands, Glob. Change Biol., 17, 2601–2614, doi:10.1111/j.1365-2486.2011.02442.x, 2011.

Merbold, L., Kutsch, W. L., Corradi, C., Kolle, O., Rebmann, C., Stoy, P. C., Zimov, S. A., and Schulze, E.-D.: Artificial drainage and associated carbon fluxes (CO_2/CH_4) in a tundra ecosystem, Glob. Change Biol., 15, 2599–2614, doi:10.1111/j.1365-2486.2009.01962.x, 2009.

Moncrieff, J., Massheder, J., deBruin, H., Elbers, J., Friborg, T., Heusinkveld, B., Kabat, P., Scott, S., Soegaard, H., and Verhoef, A.: A system to measure surface fluxes of momentum, sensible heat, water vapour and carbon dioxide, J. Hydrol., 189, 589–611, doi:10.1016/S0022-1694(96)03194-0, 1997.

Nordstroem, C., Soegaard, H., Christensen, T. R., Friborg, T., and Hansen, B. U.: Seasonal carbon dioxide balance and respiration of a high-arctic fen ecosystem in NE-Greenland, Theor. Appl. Climatol., 70, 149–166, doi:10.1007/s007040170012, 2001.

Nykänen, H., Alm, J., Lång, K., Silvola, J., and Martikainen, P. J.: Emissions of CH_4, N_2O and CO_2 from a virgin fen and a fen drained for grassland in Finland, J. Biogeogr., 22, 351–357, doi:10.1016/S1161-0301(97)00036-1, 1995.

Oechel, W., Vourlitis, G., and Hastings, S.: Cold season CO_2 emission from arctic soils, Global Biogeochem. Cy., 11, 163–172, doi:10.1029/96GB03035, 1997.

Oechel, W. C., Vourlitis, G. L., Verfaillie Jr., J., Crawford, T., Brooks, S., Dumas, E., Hope, A., Stow, D., Boynton, B., Nosov, V., and Zulueta, R.: A scaling approach for quantifying the net CO_2 flux of the Kuparuk River Basin, Alaska, Glob. Change Biol., 6, 160–173, doi:10.1046/j.1365-2486.2000.06018.x, 2000.

Ono, K., Miyata, A., and Yamada, T.: Apparent downward CO_2 flux observed with open-path eddy covariance over a non-vegetated surface, Theor. Appl. Climatol., 92, 195–208, doi:10.1007/s00704-007-0323-3, 2008.

Parmentier, F. J. W., van der Molen, M. K., van Huissteden, J., Karsanaev, S. A., Kononov, A. V., Suzdalov, D. A., Maximov, T. C., and Dolman, A. J.: Longer growing seasons do not increase net carbon uptake in the northeastern Siberian tundra, J. Geophys. Res., 116, G04013, doi:10.1029/2011JG001653, 2011.

Pihlatie, M. K., Kiese, R., Brüggemann, N., Butterbach-Bahl, K., Kieloaho, A.-J., Laurila, T., Lohila, A., Mammarella, I., Minkkinen, K., Penttilä, T., Schönborn, J., and Vesala, T.:

BGD
9, 9945–9991, 2012

Greenhouse gas fluxes in a drained peatland forest during spring frost-thaw event, Biogeosciences, 7, 1715–1727, doi:10.5194/bg-7-1715-2010, 2010.
Qian, H., Joseph, R., and Zeng, N.: Enhanced terrestrial carbon uptake in the Northern High Latitudes in the 21st century from the Coupled Carbon Cycle Climate Model Intercomparison Project model projections, Glob. Change Biol., 16, 641–656, doi:10.1111/j.1365-2486.2009.01989.x, 2010.
Rayment, M.: Closed chamber systems underestimate soil CO_2 efflux, Eur. J. Soil Sci., 51, 107–110, doi:10.1046/j.1365-2389.2000.00283.x, 2000.
Reichstein, M., Falge, E., Baldocchi, D., Papale, D., Aubinet, M., Berbigier, P., Bernhofer, C., Buchmann, N., Gilmanov, T., Granier, A., Grünwald, T., Havránková, K., Ilvesniemi, H., Janous, D., Knohl, A., Laurila, T., Lohila, A., Loustau, D., Matteucci, G., Meyers, T., Miglietta, F., Ourcival, J.-M., Pumpanen, J., Rambal, S., Rotenberg, E., Sanz, M., Tenhunen, J., Seufert, G., Vaccari, F, Vesala, T., Yakir, D., and Valentini, R.: On the separation of net ecosystem exchange into assimilation and ecosystem respiration: review and improved algorithm, Glob. Change Biol., 11, 1424–1439, doi:10.1111/j.1365-2486.2005.001002.x, 2005.
Repo, M. E., Huttunen, J. T., Naumov, A. V., Chichulin, A. V., Lapshina, E. D., Bleuten, W., and Martikainen, P. J.: Release of CO_2 and CH_4 from small wetland lakes in western Siberia, Tellus B, 59, 788–796, doi:10.1111/j.1600-0889.2007.00301.x, 2007.
Schuepp, P. H., Leclerc, M. Y., Macpherson, J. I., and Desjardins, R. J.: Footprint predictions of scalar fluxes from analytical solutions of the diffusion equation, Bound.-Lay. Meteorol., 50, 355–373, doi:10.1007/BF00120530, 1990.
Schuur, E. A. G., Vogel, J. G., Crummer, K. G., Lee, H., Sickman, J. O., and Osterkamp, T. E.: The effect of permafrost thaw on old carbon release and net carbon exchange from tundra, Nature, 459, 556–559, doi:10.1038/nature08031, 2009.
Shaver, G., Johnson, L., Cades, D., Murray, G., Laundre, J., Rastetter, E., Nadelhoffer, K., and Giblin, A.: Biomass and CO_2 flux in wet sedge tundras: Responses to nutrients, temperature, and light, Ecol. Monogr., 68, 75–97, 1998.
Shaver, G. R., Street, L. E., Rastetter, E. B., Van Wijk, M. T., and Williams, M.: Functional convergence in regulation of net CO_2 flux in heterogeneous tundra landscapes in Alaska and Sweden, J. Ecol., 95, 802–817, doi:10.1111/j.1365-2745.2007.01259.x, 2007.
Soegaard, H., Nordstroem, C., Friborg, T., Hansen, B. U., Christensen, T. R., and Bay, C.: Trace gas exchange in a high-arctic valley. 3. Integrating and scaling CO_2 fluxes from canopy to

BGD
9, 9945–9991, 2012

landscape using flux data, footprint modeling, and remote sensing, Global Biogeochem. Cy., 14, 725–744, doi:10.1029/1999GB001137, 2000.
Soegaard, H., Jensen, N. O., Boegh, E., Hasager, C. B., Schelde, K., and Thomsen, A.: Carbon dioxide exchange over agricultural landscape using eddy correlation and footprint modelling, Agr. Forest Meteorol., 114, 153–173, doi:10.1016/S0168-1923(02)00177-6, 2003.
Tape, K., Sturm, M., and Racine, C.: The evidence for shrub expansion in Northern Alaska and the Pan-Arctic, Glob. Change Biol., 12, 686–702, doi:10.1111/j.1365-2486.2006.01128.x, 2006.
Tarnocai, C., Canadell, J. G., Schuur, E. A. G., Kuhry, P., Mazhitova, G., and Zimov, S.: Soil organic carbon pools in the northern circumpolar permafrost region, Global Biogeochem. Cy., 23, GB2023, doi:10.1029/2008GB003327, 2009.
van der Molen, M. K., van Huissteden, J., Parmentier, F. J. W., Petrescu, A. M. R., Dolman, A. J., Maximov, T. C., Kononov, A. V., Karsanaev, S. V., and Suzdalov, D. A.: The growing season greenhouse gas balance of a continental tundra site in the Indigirka lowlands, NE Siberia, Biogeosciences, 4, 985–1003, doi:10.5194/bg-4-985-2007, 2007.
Vogel, J., Schuur, E. A. G., Trucco, C., and Lee, H.: Response of CO_2 exchange in a tussock tundra ecosystem to permafrost thaw and thermokarst development, J. Geophys. Res.-Biogeo., 114, G04018, doi:10.1029/2008JG000901, 2009.
Vourlitis, G. L. and Oechel, W. C.: Landscape-scale CO_2, H_2O vapour and energy flux of moist-wet coastal tundra ecosystems over two growing seasons, J. Ecol., 85, 575–590, 1997.
Vourlitis, G., Harazono, Y., Oechel, W., Yoshimoto, M., and Mano, M.: Spatial and temporal variations in hectare-scale net CO_2 flux, respiration and gross primary production of Arctic tundra ecosystems, Funct. Ecol., 14, 203–214, doi:10.1046/j.1365-2435.2000.00419.x, 2000.
Walker, M. D., Wahren, C. H., Hollister, R. D., Henry, G. H. R., Ahlquist, L. E., Alatalo, J. M., Bret-Harte, M. S., Calef, M. P., Callaghan, T. V., Carroll, A. B., Epstein, H. E., Jónsdóttir, I. S., Klein, J. A., Magnússon, B., Molau, U., Oberbauer, S. F., Rewa, S. P., Robinson, C. H., Shaver, G. R., Suding, K., N., Thompson, C. C., Tolvanen, A., Totland, Ø., Turner, P. L., Tweedie, C. E., Webber, P. J., and Wookey, P. A.: Plant community responses to experimental warming across the tundra biome, P. Natl. Acad. Sci. USA, 103, 1342–1346, doi:10.1073/pnas.0503198103, 2006.
Wohlfahrt, G., Fenstermaker, L. F., and Arnone, J. A.: Large annual net ecosystem CO_2 uptake of a Mojave Desert ecosystem, Glob. Change Biol., 14, 1475–1487, doi:10.1111/j.1365-2486.2008.01593.x, 2008.

BGD
9, 9945–9991, 2012

Zamolodchikov, D., Karelin, D., and Ivaschenko, A.: Sensitivity of tundra carbon balance to ambient temperature, Water Air Soil Poll., 119, 157–169, doi:10.1023/A:1005194613088, 2000.

Zamolodchikov, D. G. and Karelin, D. V.: An empirical model of carbon fluxes in Russian tundra, Glob. Change Biol., 7, 147–161, doi:10.1046/j.1365-2486.2001.00380.x, 2001.

Zamolodchikov, D. G., Karelin, D. V., Ivaschenko, A. I., Oechel, W. C., and Hastings, S. J.: CO_2 flux measurements in Russian Far East tundra using eddy covariance and closed chamber techniques, Tellus B, 55, 879–892, doi:10.1046/j.1435-6935.2003.00074.x, 2003.

Zimov, S., Davidov, S., Voropaev, Y., Prosiannikov, S., Semiletov, I., Chapin, M., and Chapin, F.: Siberian CO_2 efflux in winter as a CO_2 source and cause of seasonality in atmospheric CO_2, Clim. Change, 33, 111–120, 1996.

BGD

9, 9945–9991, 2012

Table 1. Monthly mean air temperatures and precipitation in 2007–2008 and in long-term (mean × SD) at Vorkuta meteorological station (67°48′ N, 64°01′ E, 172 m a.s.l.). Data from Komi Republican Center for Hydrometeorological and Environmental Monitoring. Monthly values significantly differing from the long-term means are shown in bold.

	Jan	Feb	Mar	Apr	May	Jun	Jul	Aug	Sep	Oct	Nov	Dec	Annual
Air *T* (°C)													
2007	**−11.5**	−23.6	**−10.0**	**−3.6**	−3.5	8.2	**17.8**	9.3	5.4	**0.8**	−10.0	**−12.6**	**−2.8**
2008	**−11.6**	−17.6	−15.0	−11.4	−3.2	7.4	**15.6**	9.4	4.8	−0.7	−10.9	**−10.7**	**−3.7**
1977–2006	−20.4 ± 4.7	−19.9 ± 4.9	−14.4 ± 3.6	−10.4 ± 4.6	−1.7 ± 2.6	7.5 ± 2.7	13.0 ± 2.2	9.6 ± 2.0	4.2 ± 1.7	−4.2 ± 3.2	−13.1 ± 4.8	−17.8 ± 4.2	−5.6 ± 1.4
Rain (mm)													
2007	32	13	35	39	29	66	30	62	61	**89**	33	n.a.	n.a.
2008*	n.a.	n.a.	n.a.	n.a.	n.a.	**12**	53	59	42	n.a.	n.a.	n.a.	n.a.
1977–2006	34 ± 14	36 ± 19	28 ± 12	30 ± 17	37 ± 12	55 ± 25	55 ± 26	60 ± 30	55 ± 30	58 ± 20	40 ± 13	42 ± 15	501 ± 110

* Precipitation as liquid rain measured at the Seida study site.

BGD
9, 9945–9991, 2012

Table 2. Coverage of different land cover types in the study region. The percent coverage of each land cover class (LCC) and microsite type is shown for the 98.6-km^2 QuickBird area.

LCC	Coverage (%)	Microsites studied at plot scale	Coverage (%)
Shrub tundra heath (n = 6)	35.7	Shrub tundra heath, dry (n = 3)	20.2
		", moist (n = 3)	15.4
Betula nana tundra heath (n = 3)	15.2	*Betula nana* tundra heath (n = 3)	15.2
Dry lichen tundra heath (n = 3)	7.1	Dry lichen tundra heath (n = 3)	7.1
Tundra heath LCTs (n = 12)	Total 57.9		
Tundra bog (n = 6)	23.3	Tundra bog, dry (n = 3)	15.0
		", moist (n = 3)	8.3
Bare peat (n = 3)	0.3	Bare peat (n = 3)	0.3
Dry peatland LCTs (n = 9)	Total 23.6		
Willow (n = 3)	8.7	Willow (n = 3)	8.7
Fen (n = 6)	5.7	Fen, *Carex* dominated (n = 3)	5.1
		", *Eriophorum* dominated (n = 3)	0.6
Wetland LCTs (n = 9)	Total 14.4		
Lakes (n = 3)	1.1	Lakes (n = 3)	1.1
Rivers	0.3	n.m.	
Water bodies	Total 1.4		
Deciduous forest stand	1.2	n.m.	
Spruce forest stand	1.1	n.m.	
Human-impacted tundra	0.3	n.m.	
Sand	0.2	n.m.	
Other classes	Total 2.7		
TOTAL	100	TOTAL	96.9

n = number of replicate flux measurement plots within LCC or microsite
nm = not measured

BGD
9, 9945–9991, 2012

Table 3. Summary of gross photosynthesis (GP) and ecosystem respiration (ER) models for the three main land-cover types (LCTs). Individual model equations were formulated for each microsite (GP) or chamber plot (ER). See Supplement for a more detailed model summary.

		GP model					ER model				
	LCTs	Period	Model*	*df*	r^2	RMSE	Period	Model	*df*	r^2	RMSE
Upland tundra $n = 12$	Shrub tundra heath, *Betula nana* tundra heath, Dry lichen tundra heath	2007 May–Jul 2008 Aug–Oct 2008	1 1, 3 1	58–95 77–87 58–71	0.846 0.810 0.829	0.80 1.08 0.75	2007 2008	5 5	30–37 35–40	0.607 0.760	0.64 0.42
Dry peatlands $n = 9$	Tundra bog, Bare peat	2007 May–Jul 2008 Aug–Oct 2008	1, 4 1, 3, 4 1, 4	69–101 75–92 48–74	0.892 0.910 0.888	0.68 0.93 0.75	2007 2008	5 5	32–37 34–40	0.679 0.783	0.44 0.50
Wetlands $n = 9$	Willow, Fen	2007 May–Jul 2008 Aug–Oct 2008	1, 2 1, 2 1, 2	81–82 35–78 44–66	0.834 0.906 0.858	1.71 1.91 1.58	2007 2008	5 5	28–32 32–35	0.703 0.788	0.77 0.91

* The model functions used: 1: $GP = Q \times PAR/(k + PAR) \times \exp(-0.5 \times ((T_{2cm} - T_{opt})/T_{tol})^2) \times (a + LAI)$

2: $GP = Q \times PAR/(k + PAR) \times \exp(-0.5 \times ((T_{mean} - T_{opt})/T_{tol})^2) \times (a + LAI)$

3: $GP = Q \times PAR/(k + PAR) \times T_{2cm} \times (a + LAI)$

4: $GP = Q \times PAR/(k + PAR) \times \exp(-0.5 \times ((T_{mean} - T_{opt})/T_{tol})^2) \times M$

5: $ER = R_{10} \times \exp(E_0 \times (1/56 - 1/(T_{mean} + 46)))$

Q = Maximum GP, k = PAR level at which GP reaches half of Q, T_{2cm} = Soil temperature at 2 cm, T_{mean} = Average of air temperature and T_{2cm}, T_{opt} = Temperature optimum of GP, T_{tol} = Temperature tolerance of GP, a = Correction term for LAI, M = The volumetric soil moisture, R_{10} = ER at 10 °C, E_0 = Activation energy of ER

BGD
9, 9945–9991, 2012

Table 4. Characteristics of the microsites measured with chamber technique: leaf area index (LAI), soil moisture (θ_v) and maximum active layer depth (AL_{max}). Data for LAI and θ_v are growing season means ± SE, whereas range is shown for AL (n = 3).

	LAI	WT (cm)		θ_v ($m^3\ m^{-3}$)		AL_{max} (cm)	
Microsite	2008	2007	2008	2007	2008	2007	2008
TUNDRA HEATH							
Shrub tundra heath, dry	0.26 ± 0.01	32 ± 1	28 ± 3	0.17 ± 0.00	0.13 ± 0.01	≥ 106	> 120
", moist	0.93 ± 0.23	32 ± 3	27 ± 2	0.22 ± 0.02	0.16 ± 0.01	> 120	> 120
Betula nana tundra heath	0.53 ± 0.06	28 ± 3	32 ± 2	0.16 ± 0.02	0.12 ± 0.02	> 120	> 120
Dry lichen tundra heath	0.11 ± 0.02	35 ± 2	39 ± 2	0.18 ± 0.00	0.14 ± 0.01	88 ± 4	94 ± 4
DRY PEATLANDS							
Tundra bog, dry	0.92 ± 0.13	34 ± 2	31 ± 5	0.16 ± 0.01	0.12 ± 0.01	49 ± 3	51 ± 3
", moist	0.45 ± 0.14	14 ± 1	18 ± 1	0.43 ± 0.02	0.40 ± 0.03	76 ± 2	81 ± 2
Bare peat	0.00	18 ± 3	23 ± 4	0.63 ± 0.01	0.60 ± 0.01	70 ± 1	62 ± 1
WETLANDS							
Willow	1.85 ± 0.11	0 ± 1	−1 ± 1	n.d.	n.d.	> 120	> 120
Fen, *Carex* dominated	1.17 ± 0.40	8 ± 1	8 ± 3	n.d.	n.d.	> 120	> 120
", *Eriophorum* dominated	0.17 ± 0.03	−3 ± 0	1 ± 2	n.d.	n.d.	> 120	> 120

BGD
9, 9945–9991, 2012

Table 5. Carbon dioxide balance for the intensive measuring period in 2008 and full year (October 2007–October 2008). Estimates for the EC footprint area are shown for different measuring techniques (plot scale measurements = chamber technique and lake measurements).

NEE, g C m^{-2}	EC measuring period				Full year
	Early season days 139–167	Growing season days 168–246	Late season days 247–279	Total days 139–279	(days 279/2007–279/2008)
EC footprint, 0.2–0.5 km^2					
Plot scale measurements + up-scaling with LCC	7 ± 3	−81 ± 37	4 ± 6	−70 ± 46	−32 ± 57
Plot scale measurements + up-scaling with LAI map	n.d.	−105 ± 27	n.d.	−93 ± 23	−57 ± 20
EC measurements	20 ± 4	−79 ± 35	32 ± 10	−28 ± 50	n.d.
Quickbird area, 98.6 km^2					
Plot scale measurements + up-scaling with LCC	8 ± 3	−94 ± 37	3 ± 5	−82 ± 46	−41 ± 57
Plot scale measurements + up-scaling with LAI map	n.d.	−127 ± 30	n.d.	−117 ± 26	−79 ± 22

n.d. = not determined

BGD
9, 9945–9991, 2012

Table 6. Summary of cumulative NEE and GP in different tundra ecosystems based on chamber and eddy covariance (EC) measurements and modeling. From chambers studies only those with area-integrated estimates were included. Ranges indicate the spatio-temporal variability of CO_2 fluxes.

Location	Tundra type (max. LAI)	Period (days)	Cumulative CO_2 Flux ($g\,C\,m^{-2}$)		Method	Reference
			NEE	GP		
Ny-Ålesund, Svalbard (79° N, 12° E)	high arctic heath	Jun–Sep (70–89 days)	−9 to +5		EC with modeling	Lloyd (2001)
Zackenberg, Greenland (74° N, 21° W)	high arctic heath, willows, fen (LAI = 0.2–1.1)	Jun–Aug (92 days)	−10 (−33 to −1)		EC with modeling	Soegaard et al. (2000)
		annual	**−2 (−19 to + 5)**			
	high arctic heath (LAI = 0.2–0.3)	Jun–Aug (80 days)	−23 to −1		EC	Groendahl et al. (2007)
		Jun–Aug (73 days)	−40 to −4	−95 to −54	EC	Lund et al. (2012)
Lena Delta, Russia (72° N, 127° E)	polygonal tundra	Jun–Aug (81 days)	−32	−118	EC	Kutzbach et al. (2007b)
		annual	**-19**			
Barrow, Alaska (70–71° N, 157° W)	sedge tundra	May–Sep (147 days)	−162 to −105	−215 to −147	EC	Harazono et al. (2003)
	sedge tundra, tussock tundra	Jun–Aug (92 days)	−70 to +61		EC	Kwon et al. (2006)
Indigirka, Russia (71° N, 147° E)	lowland tundra	**annual**	**−92**	**−232**	EC, chambers	van der Molen et al. (2007)
		Growing season (60–81 days)	−95 to −69	−211 to −158	EC	Parmentier et al. (2011)
Happy Valley, Alaska (69° N, 149° W)	sedge tundra, tussock tundra	Jun–Aug (81 days)	−40		EC	Vourlitis and Oechel (1997)
		Jun–Aug (92 days)	−77 to −55	−234 to −142	EC	Vourlitis et al. (2000)
Cherskii, Russia (69° N, 161° E)	tussock tundra (LAI = 1.4)	Jul–Oct (100 days)	−50 to +15		EC	Merbold et al. (2009)
		annual	**−38**		EC	Corradi et al. (2005)
Stordalen, Sweden (68° N, 19° E)	subarctic palsa mire	**annual**	**−3**		chambers	Bäckstrand et al. (2010)
Abisco, Sweden (68° N, 19° E)	fell field, heath, fen, shrub tundra	Jul–Aug (40 days)	−60 to −66 (−158 to −10)		chambers	Fox et al. (2008)
			−38 to −33		EC	
Lek Vorkuta, Russia (67° N, 63° E)	various tundra types	Jun–Aug (100 days)	−35 (−124 to +123)	n.a. (−325 to −78)	chambers	Heikkinen et al. (2004)
Chukotskiy, Russia (66° N, 171° E)	typical tundra	Jul–Oct (85 days)	−10	−96	EC, chambers	Zamolodchikov et al. (2003)
Daring Lake, Canada (65° N, 112° W)	low arctic tundra (LAI = 0.6–0.9)	May–Sep (109 days)	−111 to −32	−209 to −132	EC	Lafleur and Humphreys (2008, 2011)
Russian tundra (64–76° N, 30–172° W)	East-European tundra	**annual**	**−4**	**−334**	chambers with modeling	Zamolodchikov and Karelin (2001)
	Whole Russian tundra	**annual**	**−5**	**−207**		

BGD
9, 9945–9991, 2012

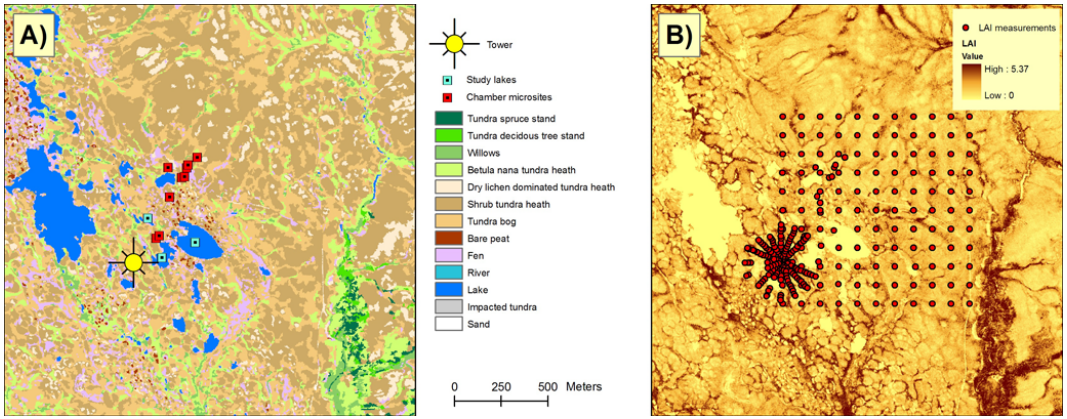

Fig. 1. (A) Land-cover classification of the study area. Location of the eddy covariance mast, chamber microsites and thermokarst lakes studied are shown on the map. **(B)** LAI map, showing the location of the LAI ground measurements.

BGD
9, 9945–9991, 2012

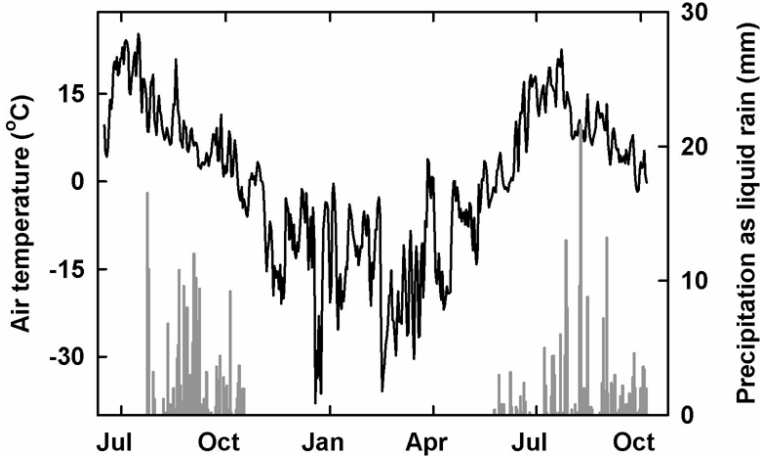

Fig. 2. Air temperature and precipitation as rain at the Seida study site in July 2007–October 2008. Precipitation was recorded during 3 July–18 October 2007 and 18 May–6 October 2008.

BGD
9, 9945–9991, 2012

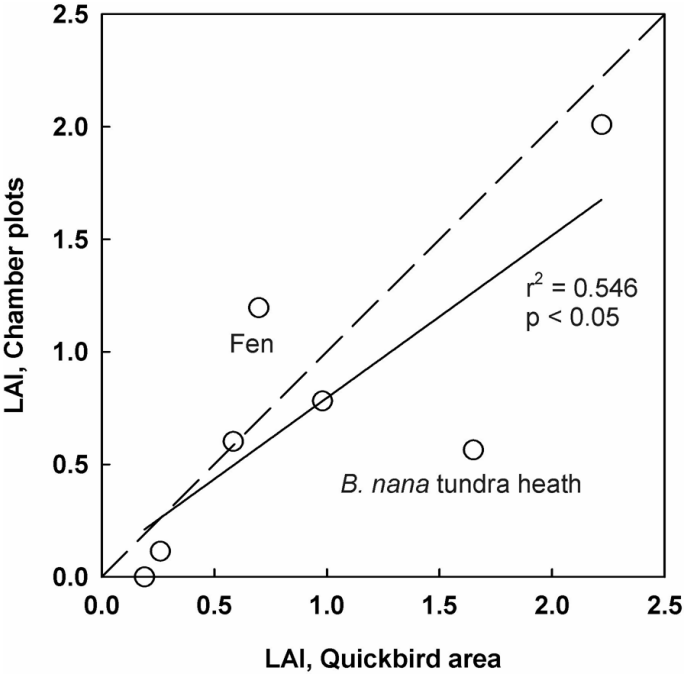

Fig. 3. Correlation of mean LAI values of different LCTs determined by two independent methods: measurements at chamber microsites and modeling based on satellite image data for the QuickBird area of 98.6 km^2.

BGD
9, 9945–9991, 2012

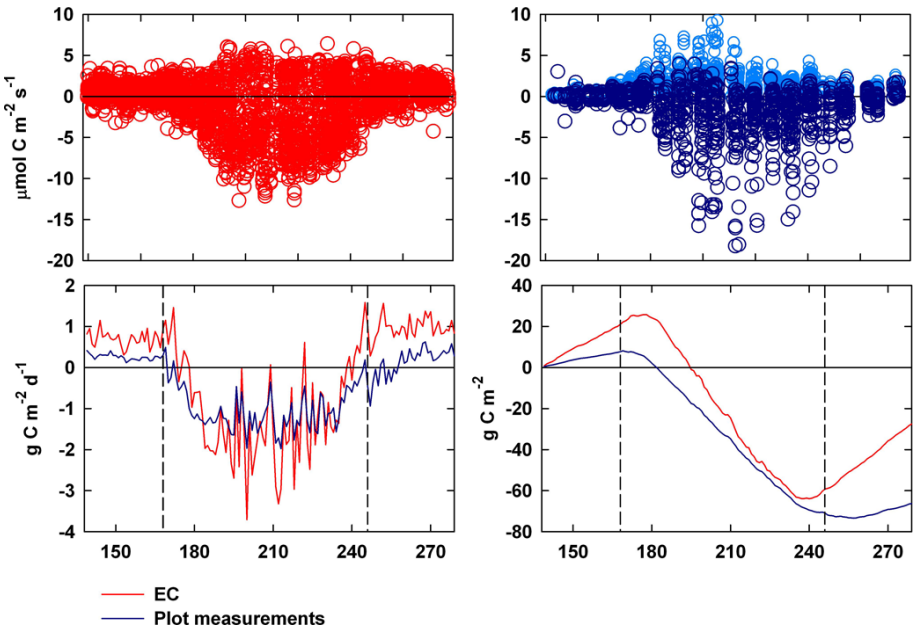

Fig. 4. Carbon dioxide fluxes of the EC footprint area in 2008 based on EC (red) and chamber measurements (blue). Top row: non-gap-filled half-hourly NEE from EC (left); raw chamber data: NEE under ambient and reduced light and ER (right). Bottom row: daily NEE fluxes by the two methods (left); cumulative NEE by the two methods (right). The daily and cumulative plot scale fluxes have been modeled and area-weighed for the EC footprint using the LCC approach. The dashed lines indicate the start and end of the growing season.

BGD
9, 9945–9991, 2012

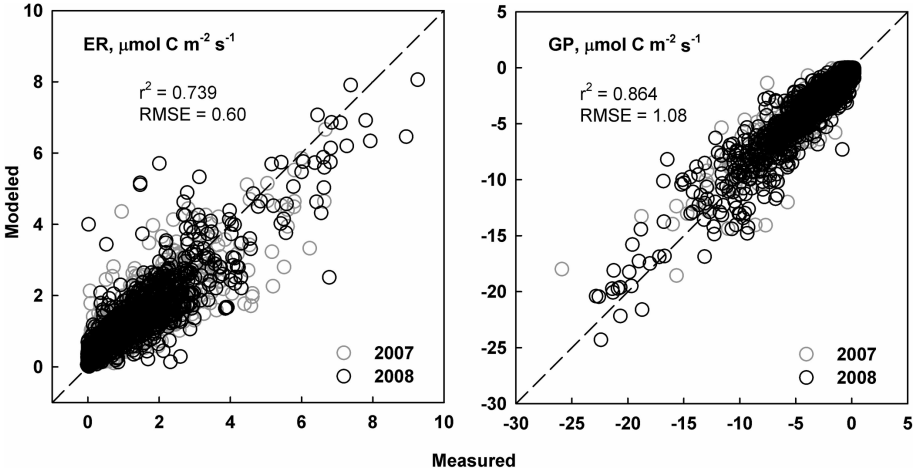

Fig. 5. Modeled vs. measured CO_2 fluxes determined by chamber technique during the two years. The r^2 and RMSE-values are shown for the entire data pool.

BGD
9, 9945–9991, 2012

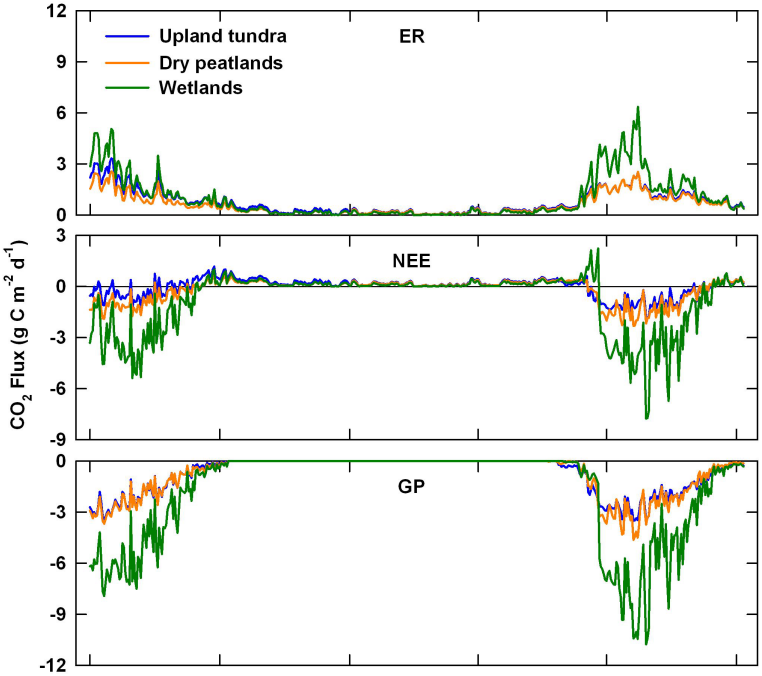

Fig. 6. Seasonal dynamics of CO_2 fluxes of the three main landscape types: upland tundra, dry peatlands and wetlands. Data are daily mean values of chamber fluxes integrated over time using empirical models.

BGD
9, 9945–9991, 2012

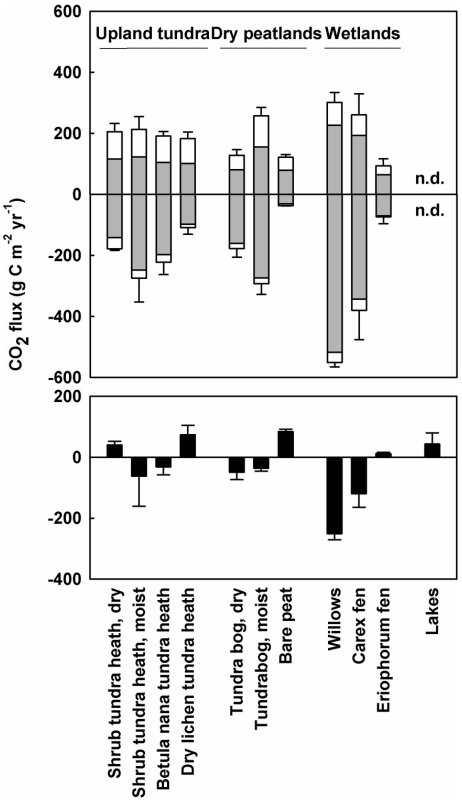

Fig. 7. The annual CO_2 balance (6 October 2007–5 October 2008) at different microsites: ER and GP (top), NEE (bottom) (mean ± SD; $n = 3$). The ER and GP components are divided into growing season and non-growing season fluxes. Positive values mean C loss from the ecosystem and negative values C uptake.

BGD
9, 9945–9991, 2012

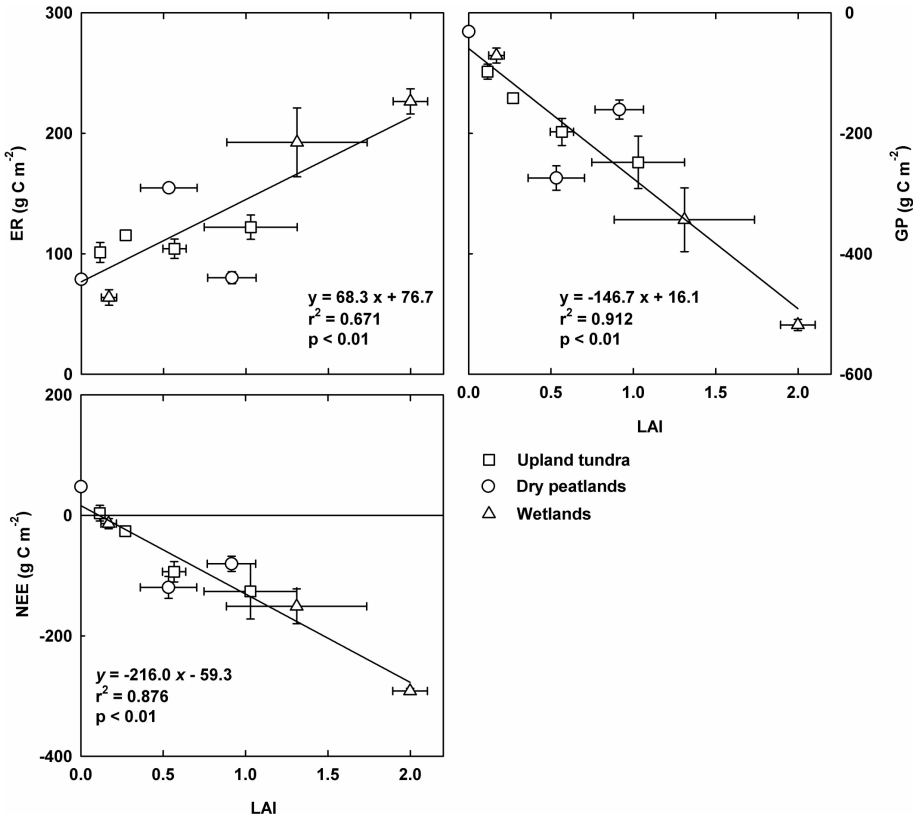

Fig. 8. Dependence between mean LAI and cumulative C fluxes for the growing season (days 168–246). Each data point represents one of the ten chamber microsites (mean ± SD; $n = 3$).

BGD
9, 9945–9991, 2012

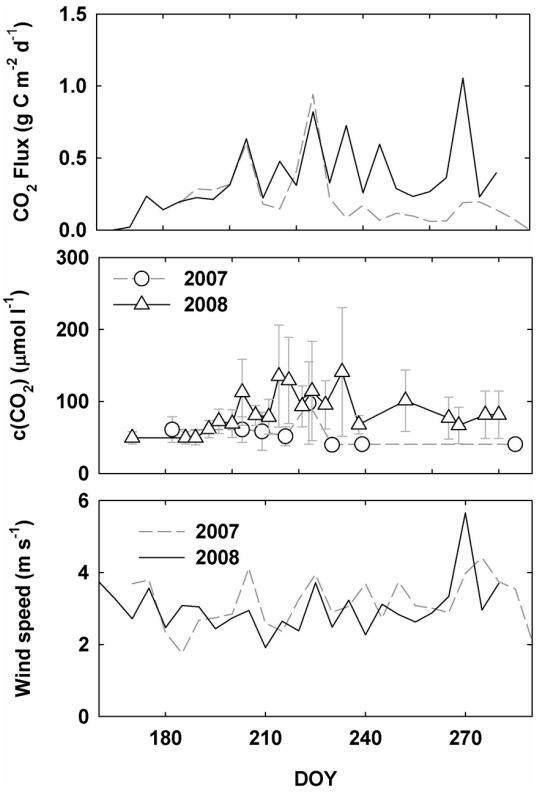

Fig. 9. CO_2 flux in thermokarst lakes during the open water period (top), CO_2 concentration in the surface water (middle) and local wind speed at 2 m (bottom) (n = 3). Flux and wind speed data are 5-day averages, whereas CO_2 concentrations in the surface water are shown for each sampling occasion (mean ± SD).

BGD
9, 9945–9991, 2012

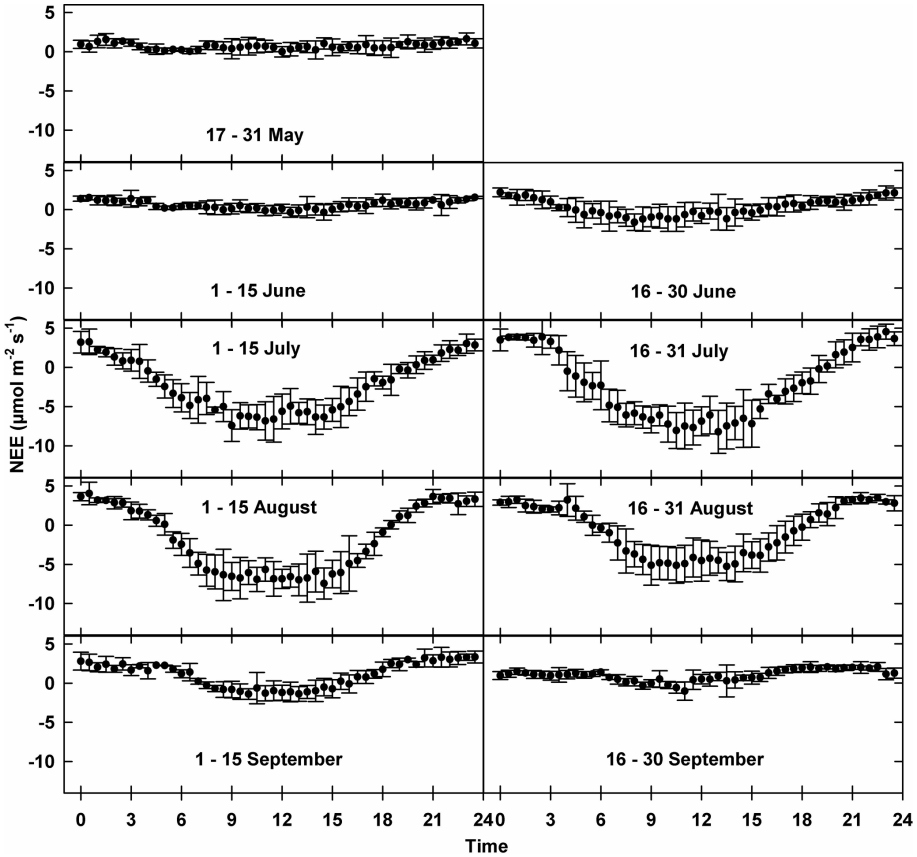

Fig. 10. Diurnal dynamics of NEE measured by EC technique. The half-hourly fluxes are averaged according to the time of the day for half-monthly periods. The error bars represent the standard deviation of the mean.

BGD
9, 9945–9991, 2012

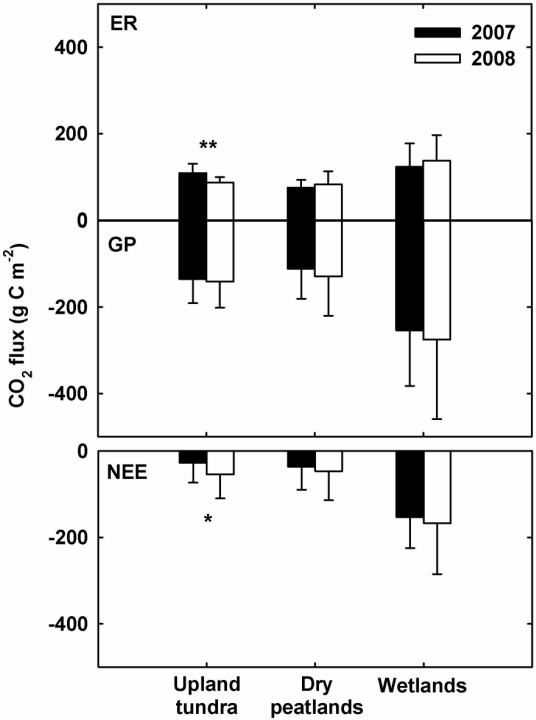

Fig. 11. Cumulative CO_2 fluxes during summer period (July–August) in the three main land-cover types in 2007 and 2008 (mean ± SD; $n = 3$). Significant differences between years are shown; ** = $p < 0.01$, * = $p < 0.05$.

BGD
9, 9945–9991, 2012

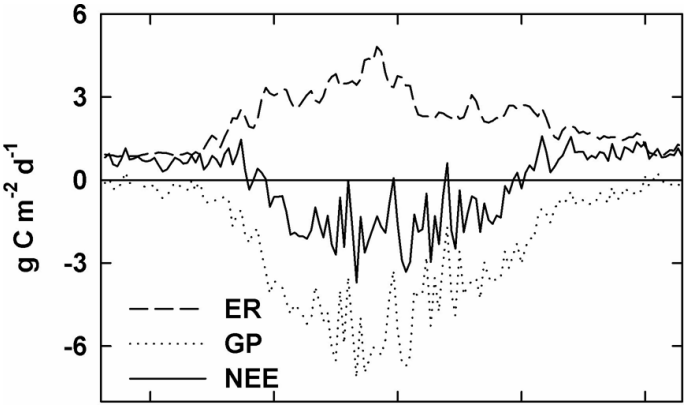

Fig. 12. Net ecosystem CO_2 exchange by EC fluxes partitioned into two components, ecosystem respiration (ER) and gross photosynthesis (GP) by modeling the respiration part. Data are daily mean values.

BGD
9, 9945–9991, 2012